JOURNAL OF GUIDANCE, CONTROL, AND DYNAMICS
Vol. 32, No. 2, March–April 2009

Engineering Notes

ENGINEERING NOTES are short manuscripts describing new developments or important results of a preliminary nature. These Notes should not exceed 2500 words (where a figure or table counts as 200 words). Following informal review by the Editors, they may be published within a few months of the date of receipt. Style requirements are the same as for regular contributions (see inside back cover).

Recursive Bias Estimation and Orbit Determination

Michael E. Hough
Raytheon Company, Woburn, Massachusetts 01801

DOI: 10.2514/1.39955

I. Introduction

ORBIT determination algorithms are designed to estimate satellite position and inertial velocity from *unbiased* sensor measurements. Static and dynamic measurement biases, which are low-frequency systematic errors, cause biases in both position *and* velocity estimates that can significantly degrade track accuracy. As only the *random* error statistics are characterized, the filter covariance usually underestimates the biased track error statistics. Track biases and covariance fidelity are important issues for correlation and fusion of multiple sensor tracks [1,2].

Many algorithms have been developed [3–10] for estimation of bias parameters in the system dynamics, in the measurements, or in both. Generally, bias parameters are estimated jointly with the position and velocity states. Depending on the number of bias parameters, this approach can be computationally intensive, the system covariance matrix can become ill conditioned, and bias-state observability and separability can be problematic. Alternatively, two-step techniques extract bias parameters from the track measurement residuals.

For current radar systems, measurement biases are calibrated by tracking one metric satellite having an accurate ephemeris, or by tracking many satellites with less accurate ephemerides [9]. Range and angle biases are calibrated *after* (not during) the data collection (s). A noteworthy exception is a real-time algorithm for angle bias estimation in wideband radars [10].

In this Note, an iterated 12-state extended Kalman filter EKF(12) is formulated for *simultaneous* (real-time) orbit determination and bias estimation. Orbit position and velocity states are augmented with six dynamic (rather than static) bias states that model radar orientation biases and radar range-angle measurement biases. Bias-state observability and separability are enhanced by physical models for the bias dynamics and by careful characterization of bias effects in the measurement residuals. For example, random and certain environmental (i.e., tropospheric) bias errors are intrinsic to the radar measurements, whereas radar orientation biases corrupt the transformation of the prior position estimate from inertial to radar coordinates. Performance evaluations will demonstrate accurate real-time state estimates and excellent covariance fidelity, which are essential for radar-to-radar track correlation and fusion.

Received 22 July 2008; revision received 8 October 2008; accepted for publication 11 October 2008.

II. Sensor Models

Radars provide accurate three-dimensional position measurements for orbit determination. Distance (or time delay) is measured relative to the radar, and directional (or angle) measurements are reported in Cartesian radar-face coordinates. For radars on moving platforms, position, velocity, orientation, and angular rate of the radar array are provided by a strapdown inertial navigation system (INS) mounted on the radar face.

A phased-array radar using a linear FM ("chirp") waveform measures a linear combination $\rho_m = \rho + \tau_{\mathrm{RD}}\dot{\rho}$ of range distance ρ and range rate $\dot{\rho}$. The range-Doppler coupling time τ_{RD} depends on radar center frequency, pulse length, chirp bandwidth, and chirp polarity [11]. As τ_{RD} is known, ρ and $\dot{\rho}$ could be measured directly by transmitting two virtually simultaneous pulses with positive and negative τ_{RD} values, or these quantities can be determined by track processing of ρ_m. Range-Doppler radars can also provide direct measurements of $\dot{\rho}$, but these measurements are not considered here.

Radar angle measurements, which are determined using monopulse techniques [12], provide azimuthal and vertical direction cosines u and v, respectively, of the unit line-of-sight (LOS) vector $\boldsymbol{\lambda}$ in Cartesian radar-face coordinates:

$$\boldsymbol{\lambda} = [\,w \quad u \quad v\,]^T \qquad w = \sqrt{1 - u^2 - v^2}$$

where w is specified by $|\boldsymbol{\lambda}| = 1$. A mechanical control system steers the radar array in azimuth and elevation to maintain an orbiting target within a few degrees of radar boresight, and an electronic steering control system centers the radar beam on the object. It follows that $w \equiv 1, u = v = 0$ when the LOS is *at* radar boresight, and $0 < w < 1$ otherwise.

Radar range and angle biases $\delta\boldsymbol{\eta} = [\,\delta\rho \quad \delta u \quad \delta v\,]^T$ are modeled as the sum of static and dynamic error components $\delta\boldsymbol{\eta} = \delta\boldsymbol{\eta}_S + \delta\boldsymbol{\eta}_D$ in radar-face coordinates. Dynamic bias errors $\delta\boldsymbol{\eta}_D$ arise primarily from *uncompensated* tropospheric refraction errors, which fluctuate with LOS elevation and local atmospheric conditions along the radar ray to the target [13–16]. Static or time-invariant biases include constant, scale factor, and misalignment terms:

$$\delta\boldsymbol{\eta}_S = \begin{bmatrix} \delta\rho_B + \kappa_\rho\rho \\ \delta u_B + \kappa_u u - \delta\varphi v \\ \delta v_B + \kappa_v v + \delta\varphi u \end{bmatrix}$$

where $\delta\rho_B$, δu_B, and δv_B are constant biases, κ_ρ, κ_u, and κ_v are scale factor biases, and $\delta\varphi$ is a "clock error" measured around the radar boresight. Constant biases are usually removed during the radar calibration process. Although scale factor and misalignment biases can become significant at large off-boresight scan angles, these errors may be neglected when the radar LOS is near boresight (i.e., $u, v \approx 0$). As all static biases can be neglected for the stated reasons, the radar bias states are hereafter the same as the dynamic biases ($\delta\boldsymbol{\eta} = \delta\boldsymbol{\eta}_D$).

The radar INS reports orientation as a yaw angle ψ measured from the east in the local horizontal plane, a pitch angle ϑ measured up from the local horizontal to the radar boresight, and a roll angle ϕ measured around radar boresight. The transformation matrix $\Re$ from the inertial frame to radar-face coordinates is specified by

$$\Re(\phi, \vartheta, \psi) = \Re_1(\phi)\Re_2(-\vartheta)\Re_3(\psi)\Re_s(\alpha_s, L_s)$$

where numerical subscripts $\Re_j$ identify the axis of rotation. The transformation $\Re_s(\alpha_s, L_s)$ from the inertial frame to topocentric east–north–up (ENU) coordinates at the radar depends on the radar right ascension α_s and geodetic latitude L_s.

INS navigation and orientation biases arise from gyro and accelerometer bias, scale factor, and drift errors. The INS is erected to local vertical and aligned to the north using a conventional *gyrocompassing* alignment procedure. Horizontal (north-pointing) misalignments cause a yaw bias $\delta\psi$, whereas vertical misalignments cause both a pitch bias $\delta\vartheta$ and a roll bias $\delta\phi$. For a Global Positioning System-aided INS, navigation accuracy is precise and errors in α_s and L_s may be neglected.

III. Nonlinear Prediction Models

The filter state vector $\mathbf{x}$ includes the inertial position $\mathbf{r}$ of the satellite, its inertial velocity $\mathbf{v}$, INS orientation biases $\delta\boldsymbol{\xi}$, and radar measurement biases $\delta\boldsymbol{\eta}$:

$$\mathbf{x} = \begin{bmatrix} \mathbf{r}^T(t) & \mathbf{v}^T(t) & \delta\boldsymbol{\xi}^T(t) & \delta\boldsymbol{\eta}^T(t) \end{bmatrix}^T \qquad \mathbf{r} = [\,x \quad y \quad z\,]^T$$
$$\mathbf{v} = [\,\dot{x} \quad \dot{y} \quad \dot{z}\,]^T \qquad \delta\boldsymbol{\xi} = [\,\delta\psi \quad \delta\theta \quad \delta\phi\,]^T$$
$$\delta\boldsymbol{\eta} = [\,\delta\rho \quad \delta u \quad \delta v\,]^T$$

ENU orientation biases include a yaw bias $\delta\psi$, a pitch bias $\delta\vartheta$, and a roll bias $\delta\phi$. Radar measurement biases include a range bias $\delta\rho$ and direction-cosine biases δu and δv.

At altitudes above 500 km where drag is not important, orbital motion is described by

$$\frac{\mathrm{d}\mathbf{r}}{\mathrm{d}t} = \mathbf{v}$$
$$\frac{\mathrm{d}\mathbf{v}}{\mathrm{d}t} = -\frac{\mu_e}{r^2}\left\{\frac{\mathbf{r}}{r} - \frac{3J_2R_e^2}{2r^2}\left[\left(\frac{5z^2}{r^2} - 1\right)\frac{\mathbf{r}}{r} - \frac{2z}{r}\hat{Z}\right]\right\} + \nabla U$$

where μ_e, R_e, and $\hat{Z}$ are the Earth's gravitational parameter, equatorial radius, and unit-polar axis, respectively, and time derivatives are taken with respect to the Earth-centered inertial (ECI) frame. The dominant gravitational accelerations arise from the central, inverse-square gravity field and from Earth oblateness (modeled by the J_2 coefficient). As each higher-order zonal or tesseral harmonic term of the geopotential function U is $\mathcal{O}(J_2^2)$, the higher-order disturbing acceleration ∇U is at most 15–20 μg at orbital altitudes of 700 km, depending on the geographic location of the subsatellite point. For short data collection and prediction intervals, ∇U may be neglected.

INS orientation biases fluctuate as the radar array (on which the INS is mounted) follows the satellite trajectory in elevation and azimuth. Differential equations may be derived by linearization of the Euler equations specifying the angular rates:

$$\frac{\mathrm{d}}{\mathrm{d}t}(\delta\boldsymbol{\xi}) = \Lambda(\theta,\phi)\delta\boldsymbol{\xi} + \Im^{-1}\delta\boldsymbol{\omega}_s$$
$$\Lambda(\theta,\phi,\boldsymbol{\omega}_s) = \begin{bmatrix} \frac{\partial\Im^{-1}}{\partial\psi}\boldsymbol{\omega}_s & \frac{\partial\Im^{-1}}{\partial\theta}\boldsymbol{\omega}_s & \frac{\partial\Im^{-1}}{\partial\phi}\boldsymbol{\omega}_s \end{bmatrix}$$
$$\Im^{-1}(\theta,\phi) = \frac{1}{\cos\theta}\begin{bmatrix} 0 & \sin\phi & \cos\phi \\ 0 & -\cos\theta\cos\phi & \cos\theta\sin\phi \\ \cos\theta & -\sin\theta\sin\phi & -\sin\theta\cos\phi \end{bmatrix}$$
$$\frac{\partial\Im^{-1}}{\partial\psi} = O_3$$
$$\frac{\partial\Im^{-1}}{\partial\theta} = \frac{1}{\cos\theta}\begin{bmatrix} 0 & 0 & 0 \\ 0 & \sin\theta\cos\phi & -\sin\theta\sin\phi \\ -\sin\theta & -\cos\theta\sin\phi & -\cos\theta\cos\phi \end{bmatrix} + \tan\theta\Im^{-1}$$
$$\frac{\partial\Im^{-1}}{\partial\phi} = \frac{1}{\cos\theta}\begin{bmatrix} 0 & \cos\phi & -\sin\phi \\ 0 & \cos\theta\sin\phi & \cos\theta\cos\phi \\ 0 & -\sin\theta\cos\phi & \sin\theta\sin\phi \end{bmatrix}$$

where $\boldsymbol{\omega}_s$ and $\delta\boldsymbol{\omega}_s$ are the Earth-relative angular rate and its bias error in radar-face coordinates. The rate bias $\delta\boldsymbol{\omega}_s$ is a zero-mean, Gaussian random vector with statistics:

$$E\{\delta\boldsymbol{\omega}_s\} = \mathbf{0}_3, \qquad E\{\delta\boldsymbol{\omega}_s\delta\boldsymbol{\omega}_s^T\} = \begin{bmatrix} q_\omega & 0 & 0 \\ 0 & q_\omega & 0 \\ 0 & 0 & q_\omega \end{bmatrix}$$

Radar measurement biases fluctuate with local atmospheric conditions along the radar ray. Dynamic bias errors are modeled by a linear, first-order Markov model:

$$\frac{\mathrm{d}}{\mathrm{d}t}(\delta\boldsymbol{\eta}) + \frac{1}{\tau_A}\delta\boldsymbol{\eta} = \frac{1}{\tau_A}\delta\mathbf{f}$$

where the disturbance input $\delta\mathbf{f}$ is a zero-mean, Gaussian random vector with statistics:

$$E\{\delta\mathbf{f}\} = \mathbf{0}_3, \qquad E\{\delta\mathbf{f}\delta\mathbf{f}^T\} = \begin{bmatrix} q_\rho & 0 & 0 \\ 0 & q_{uv} & 0 \\ 0 & 0 & q_{uv} \end{bmatrix}$$

The constant variances q_ρ and q_{uv} may be interpreted as process noise "commands" to the covariance equations of the first-order Markov dynamic bias model. The Markov time constant τ_A varies with LOS elevation γ, with elevation rate $\dot{\gamma}$, and with the elevation-dependent refraction error $\varepsilon(\gamma)$ and its elevation gradient (refer to the Appendix):

$$\tau_A = -\frac{\varepsilon(\gamma)}{\dot{\gamma}\,\mathrm{d}\varepsilon/\mathrm{d}\gamma}$$

As $\frac{\mathrm{d}\varepsilon}{\mathrm{d}\gamma} < 0$, stable error dynamics ($\tau_A > 0$) occur with increasing elevation ($\dot{\gamma} > 0$) and unstable error dynamics ($\tau_A < 0$) occur with decreasing elevation ($\dot{\gamma} < 0$). Although τ_A is undefined at the peak elevation because $\dot{\gamma} = 0$, a maximum positive τ_A value is assigned to avoid singularities.

The covariance prediction equations are given by

$$\frac{\mathrm{d}P}{\mathrm{d}t} = F(\mathbf{x})P + PF(\mathbf{x})^T + GQG^T$$
$$F(\mathbf{x}) = \begin{bmatrix} O_3 & I_3 & O_3 & O_3 \\ \Gamma & O_3 & O_3 & O_3 \\ O_3 & O_3 & \Lambda & O_3 \\ O_3 & O_3 & O_3 & -(1/\tau_A)I_3 \end{bmatrix}$$
$$G = \begin{bmatrix} O_3 & O_3 & O_3 & O_3 \\ O_3 & I_3 & O_3 & O_3 \\ O_3 & O_3 & \Im^{-1} & O_3 \\ O_3 & O_3 & O_3 & (1/\tau_A)I_3 \end{bmatrix}$$

where the gravity-gradient matrix Γ is complete to $\mathcal{O}(J_2)$:

$$\Gamma = \frac{\partial\mathbf{g}}{\partial\mathbf{r}^T} = \frac{\mu_e}{r^3}\left(\frac{3\mathbf{r}\mathbf{r}^T}{r^2} - I_3\right) + \frac{3\mu_e J_2 R_e^2}{2r^5}\Gamma_2$$
$$\Gamma_2 = \begin{bmatrix} \frac{5(x^2+z^2)}{r^2} - \frac{35x^2z^2}{r^4} - 1 & \frac{5xy}{r^2} - \frac{35xyz^2}{r^4} & \frac{15xz}{r^2} - \frac{35xz^3}{r^4} \\ \frac{5xy}{r^2} - \frac{35xyz^2}{r^4} & \frac{5(y^2+z^2)}{r^2} - \frac{35y^2z^2}{r^4} - 1 & \frac{15yz}{r^2} - \frac{35yz^3}{r^4} \\ \frac{15xz}{r^2} - \frac{35xz^3}{r^4} & \frac{15yz}{r^2} - \frac{35yz^3}{r^4} & \frac{30z^2}{r^2} - \frac{35z^4}{r^4} - 3 \end{bmatrix}$$

State estimation errors $\delta\hat{\mathbf{x}}$ cause errors in $F(\mathbf{x})$ that are not represented in the linear equations for covariance prediction. Consequently, process noise Q is added to improve covariance fidelity, to prevent premature filter convergence, and to improve numerical conditioning of P. A diagonal Q matrix is assigned with constant velocity variance q_v, constant INS angular-rate variance q_ω, constant range dynamic bias variance q_ρ, and constant u, v dynamic bias variance q_{uv}:

$$Q = \mathrm{diag}\{0 \;\; 0 \;\; 0 \;\; q_v \;\; q_v \;\; q_v \;\; q_\omega \;\; q_\omega \;\; q_\omega \;\; q_\rho \;\; q_{uv} \;\; q_{uv}\}$$

Table 1 EKF(12) process noise model

Description	Symbol	Value
RMS velocity process noise (each axis)	q_v	0 m^2/s^3
INS angular velocity process noise (each axis)	q_ω	(2 μrad/s)^2
Dynamic range bias process noise command	q_ρ	(10 m)^2
Dynamic u, v bias process noise command (each axis)	q_{uv}	(1000 μrad)^2

Numerical values of these parameters are provided in Table 1 for an update rate of 1 Hz.*

IV. Measurement Functions

Bias-state observability and separability properties are crucially dependent on the mathematical models for the bias influence in the measurement residual and in the measurement sensitivity matrix used for the filter gain matrix. The true radar measurement $\mathbf{y}$ is specified in radar-face spherical coordinates:

$$\mathbf{y} = [\,\rho + \tau_{\mathrm{RD}}\dot{\rho} \quad u \quad v\,]^T + \delta\boldsymbol{\eta} + \boldsymbol{\upsilon}$$
$$R = E\{\boldsymbol{\upsilon}\boldsymbol{\upsilon}^T\} = \mathrm{diag}\{\,\sigma^2_{\rho+\tau\dot{\rho}} \quad \sigma^2_u \quad \sigma^2_v\,\}$$

Radar measurements are corrupted by additive measurement bias errors $\delta\boldsymbol{\eta}$ and by zero-mean, uncorrelated Gaussian random errors $\boldsymbol{\upsilon}$ with a diagonal measurement noise matrix R. It is important to note that $\mathbf{y}$ is independent of the orientation bias $\delta\boldsymbol{\xi}$.

Prior estimates of the radar measurements are determined from radar position and inertial velocity $\mathbf{R}_s$ and $\mathbf{V}_s$, prior orbit estimates $\bar{\mathbf{r}}$ and $\bar{\mathbf{v}}$, and the transformation $\bar{\Re}$ which contains the orientation biases:

$$\bar{\boldsymbol{\rho}} = \bar{\mathbf{r}} - \mathbf{R}_s, \qquad \bar{\rho} = |\bar{\boldsymbol{\rho}}| \qquad \bar{\boldsymbol{\lambda}} = [\,\bar{w} \quad \bar{u} \quad \bar{v}\,]^T = \frac{1}{\bar{\rho}}\bar{\Re}\,\bar{\boldsymbol{\rho}}$$
$$\dot{\bar{\rho}} = [\bar{\Re}(\bar{\mathbf{v}} - \mathbf{V}_s)]^T\bar{\boldsymbol{\lambda}}$$

The estimated radar measurement $\bar{\mathbf{y}}$ depends on $\bar{\rho}$, $\dot{\bar{\rho}}$, $\bar{u}$, and $\bar{v}$ and prior estimates of the orientation and measurement biases $\delta\bar{\boldsymbol{\xi}}$ and $\delta\bar{\boldsymbol{\eta}}$:

$$\bar{\mathbf{y}} = h(\bar{\mathbf{x}}) = \mathbf{h}_0(\bar{\mathbf{r}}, \bar{\mathbf{v}}) - J_\xi\delta\bar{\boldsymbol{\xi}} + \delta\boldsymbol{\eta} \qquad \mathbf{h}_0 = [\,\bar{\rho} + \tau_{\mathrm{RD}}\dot{\bar{\rho}} \quad \bar{u} \quad \bar{v}\,]^T$$
$$J_\xi = \frac{\partial(\rho + \tau_{\mathrm{RD}}\dot{\rho}, u, v)}{\partial(\psi, \theta, \phi)}$$
$$\frac{\partial(\rho + \tau_{\mathrm{RD}}\dot{\rho})}{\partial(\psi, \theta, \phi)} = -\frac{1}{2}\bar{\rho}[\cos^2\bar{\theta}\delta\bar{\psi} \quad \delta\bar{\theta} \quad 0\,]$$

where $\partial(u, v)/\partial(\psi, \theta, \phi)$ is specified by selection of the appropriate rows of the 3×3 Jacobian matrix:

$$\frac{\partial(w, u, v)}{\partial(\psi, \theta, \phi)} = \Omega(\bar{\boldsymbol{\lambda}})\bar{\Im}$$

As orientation bias "measurements" are implicit in $\mathbf{h}_0$, the $J_\xi\delta\bar{\boldsymbol{\xi}}$ term is *subtracted*† from (rather than added to) $\mathbf{h}_0$, because $\mathbf{y}$ is independent of $\delta\bar{\boldsymbol{\xi}}$ (as noted earlier). Finally, orientation biases cause second-order range corrections which are always negative [i.e., effectively a $\cos(\,\cdot\,) - 1$ term] because $\bar{\rho}$ is projected onto a misaligned unit LOS direction. As range is independent of $\delta\bar{\boldsymbol{\xi}}$ to first order, this second-order term provides *mathematical* observability of the yaw orientation bias, although this term is not advantageous unless high precision wideband range measurements are available.

The linearized measurement sensitivity matrix is determined by partial differentiation of the measurement function with respect to the state variables:

$$C(\mathbf{x}) = \begin{bmatrix} \frac{\partial\mathbf{h}_0}{\partial\mathbf{r}^T} & \frac{\partial\mathbf{h}_0}{\partial\mathbf{v}^T} & -J_\xi & I_3 \end{bmatrix} \qquad \frac{\partial\mathbf{h}_0}{\partial\mathbf{r}^T} = \frac{\partial(\rho, u, v)}{\partial(x, y, z)}$$
$$\frac{\partial\mathbf{h}_0}{\partial\mathbf{v}^T} = \begin{bmatrix} \tau_{\mathrm{RD}}\partial\dot{\rho}/\partial(\dot{x}, \dot{y}, \dot{z}) \\ O_{2\times3} \end{bmatrix}$$

Partial derivatives of $\mathbf{h}_0$ appearing in $C(\mathbf{x})$ are selected from the appropriate rows and columns of the 4×3 Jacobian transformation matrix:

$$\frac{\partial(\rho, w, u, v)}{\partial(x, y, z)} = \frac{\partial(\dot{\rho}, \dot{w}, \dot{u}, \dot{v})}{\partial(\dot{x}, \dot{y}, \dot{z})} = \begin{bmatrix} \boldsymbol{\lambda}^T\Re \\ \frac{1}{\rho}(I_3 - \boldsymbol{\lambda}\boldsymbol{\lambda}^T)\Re \end{bmatrix}$$

V. Iterated Batch Filter Initialization

EKF(12) must be initialized at radar acquisition t_0 with prior estimates of the state vector and covariance matrix. When prior information (e.g., from other sensors) is not available, an initial state estimate and covariance may be determined with a batch filter using radar detections collected on a short time interval $t \in [\,t_0 \quad t_m\,]$. Earlier work [17] has shown that a batch filter provides accurate estimates to promote linear error response of the recursive filter, and properly correlated covariances that accelerate filter error convergence. Although unnecessary for an isolated satellite track, a preliminary returns-to-track association process is necessary for track initialization on multiple objects.

The nonlinear batch estimation process is iterated to improve estimation accuracy and covariance fidelity. This process begins with initial estimates $\bar{\mathbf{r}}_0$, $\bar{\mathbf{v}}_0$ and covariance $\bar{M}_0$ generated with a polynomial-batch fit to the radar detections data:

$$\hat{\mathbf{x}}_0^{(1)} = \begin{bmatrix} \hat{\mathbf{r}}_0 \\ \hat{\mathbf{v}}_0 \\ \mathbf{0}_6 \end{bmatrix}, \qquad \hat{M}_0^{(1)} = \begin{bmatrix} \bar{M}_0 + M_B & O_{6\times6} \\ O_{6\times6} & D_B \end{bmatrix}$$

As the initial biases are unknown, prior bias estimates are zero, and prior bias statistics are modeled by a 6×6 diagonal bias covariance matrix D_B (refer to Table 2). As $\hat{\mathbf{r}}_0$ and $\hat{\mathbf{v}}_0$ contain biases because the measurements are biased, $\bar{M}_0$ is inflated with a 6×6 ECI bias covariance matrix M_B that is consistent with D_B.

Orientation bias statistics are based on typical INS erection and alignment uncertainties (Table 2) showing that the yaw (or alignment) uncertainty is larger than the pitch and roll (or erection) uncertainties. Ruv dynamic bias statistics are typical tropospheric refraction uncertainties at low elevations (<5°) and for a 10% compensation error. Although tropospheric azimuth uncertainties are usually small relative to elevation uncertainties, the same uncertainties are assigned to the dynamic u and v biases.

Maximum-likelihood estimates of initial EKF(12) state $\hat{\mathbf{x}}_0$ and the corresponding covariance matrix $\hat{M}_0$ are determined with an iterated batch filter:

$$\hat{M}_0^{(i+1)} = [(\hat{M}_0^{(1)})^{-1} + (H^TW^{-1}H)^{-1}]^{-1}$$
$$\hat{\mathbf{x}}_0^{(i+1)} = \hat{\mathbf{x}}_0^{(i)} + \hat{M}_0^{(i+1)}H^TW^{-1}\begin{bmatrix} \hat{\mathbf{y}}_0 - \hat{\mathbf{h}}(\hat{\mathbf{x}}_0^{(i)}) \\ \hat{\mathbf{y}}_1 - \hat{\mathbf{h}}(\hat{\mathbf{x}}_1^{(i)}) \\ \vdots \\ \hat{\mathbf{y}}_m - \hat{\mathbf{h}}(\hat{\mathbf{x}}_m^{(i)}) \end{bmatrix}$$

Table 2 Initial bias-state covariances

Bias-state description	1σ value
Yaw orientation bias	(150 μrad)^2
Pitch & roll orientation bias (each axis)	(80 μrad)^2
Dynamic range bias	(5 m)^2
Dynamic u, v bias (each axis)	(500 μrad)^2

*Lower process noise values (not provided here) are recommended at higher data rates to assure satisfactory disturbance rejection.

†Equivalently, this term is added to $\mathbf{y}$ (because it is otherwise independent of orientation biases) when the measurement residual is formed.

$$H = \begin{bmatrix} C(\hat{\mathbf{x}}_0^{(i)})\Phi(\hat{\mathbf{x}}_0^{(i)}, 0) \\ C(\hat{\mathbf{x}}_1^{(i)})\Phi(\hat{\mathbf{x}}_0^{(i)}, t_1 - t_0) \\ \vdots \\ C(\hat{\mathbf{x}}_m^{(i)})\Phi(\hat{\mathbf{x}}_0^{(i)}, t_m - t_0) \end{bmatrix}$$

$$W^{-1} = \begin{bmatrix} N_0^{-1} & O_3 & \cdots & O_3 \\ O_3 & N_1^{-1} & \cdots & O_3 \\ \vdots & \vdots & \ddots & \vdots \\ O_3 & O_3 & \cdots & N_m^{-1} \end{bmatrix}$$

$$N_n = C(\hat{\mathbf{x}}_n^{(i)})\hat{M}_n^{(i)}C^T(\hat{\mathbf{x}}_n^{(i)}) + R_n$$

where superscript i denotes iteration number and subscripts indicate time t_n $(0 \le n \le m)$. Successive estimates $\hat{\mathbf{x}}_0^{(i)}$ change on each iteration $(i > 1)$, but the prior covariance $\hat{M}_0^{(1)}$ is not changed to prevent overly optimistic covariances. On each iteration, initial estimates and covariances from the preceding iteration step are predicted from t_0 to t_n by numerical integration of the state and covariance prediction equations and the following matrix-differential equation for the state transition matrix:

$$\dot{\Phi} = F(\hat{\mathbf{x}})\Phi$$

Alternatively, discrete-time covariance prediction may be performed using Φ:

$$\hat{M}_n^{(i)} = \Phi(\hat{\mathbf{x}}_0^{(i)}, t_n - t_0)\hat{M}_0^{(i)}\Phi^T(\hat{\mathbf{x}}_0^{(i)}, t_n - t_0)$$

Batch estimates and covariances are iterated (at most) 5 times, using the same set of detections. At least 25 to 50 detections are needed for a properly conditioned covariance matrix for EKF(12).

VI. Iterated Recursive Estimates and Covariances

For each reported detection, EKF(12) updates are iterated to mitigate the effects of measurement nonlinearities arising from ECI state estimates. Alternatively, iteration would not have been necessary for updates in radar range-angle coordinates or for range-angle measurements transformed to Cartesian face coordinates [18]. Care must be exercised with the first approach because the transformations to range-angle coordinates and back to ECI coordinates (for prediction) essentially add and subtract INS biases in a self-canceling way, thereby compromising observability.

Using superscripts to indicate the iteration number and subscripts to indicate the time t_n, the iteration process begins with a prior estimate and covariance:

$$\hat{\mathbf{x}}_n^{(1)} = \bar{\mathbf{x}}_n, \qquad P_n^{(1)} = M_n$$

The initial estimate and covariance $\bar{\mathbf{x}}_0$ and M_0 (i.e., at acquisition time t_0) are provided by the batch initialization process. On subsequent updates, $\bar{\mathbf{x}}_0$ and M_0 are specified by the predictions from the previous recursive update step. For $i \ge 1$, the nonlinear functions $C_n^{(i)} = C(\hat{\mathbf{x}}_n^{(i)})$ and $\mathbf{h}(\hat{\mathbf{x}}_n^{(i)})$ are evaluated with the prior estimate, as are the following:

$$\boldsymbol{\varepsilon}_n^{(i)} = \mathbf{y}_n - \mathbf{h}(\hat{\mathbf{x}}_n^{(i)}) - C_n^{(i)}(\bar{\mathbf{x}}_n - \hat{\mathbf{x}}_n^{(i)})$$

$$N_n^{(i)} = C_n^{(i)}M_n(C_n^{(i)})^T + R_n \qquad K_n^{(i)} = M_n(C_n^{(i)})^T(N_n^{(i)})^{-1}$$

The EKF(12) state estimate and covariance are then updated:

$$\hat{\mathbf{x}}_n^{(i+1)} = \bar{\mathbf{x}}_n + K_n^{(i)}\boldsymbol{\varepsilon}_n^{(i)}$$

$$P_n^{(i+1)} = K_n^{(i)}R_n(K_n^{(i)})^T + [I_{12} - K_n^{(i)}C_n^{(i)}]M_n[I_{12} - K_n^{(i)}C_n^{(i)}]^T$$

State estimation accuracy and covariance fidelity improve with each iteration, provided the state variables are sufficiently observable [19]. The first iteration $(i = 1)$ is the conventional EKF update because $\boldsymbol{\varepsilon}_n^{(1)} = \mathbf{y}_n - \mathbf{h}(\hat{\mathbf{x}}_n^{(1)})$ (i.e., the correction term is zero). Nonlinearities may cause differences in the statistics of $\boldsymbol{\varepsilon}_n^{(1)}$ and its covariance $N_n^{(1)}$. As $P_n^{(1)}$ is based on $N_n^{(1)}$, $P_n^{(1)}$ may have poor *covariance fidelity* because it may not accurately represent the statistics of the estimation errors. On subsequent iterations $(i \ge 2)$, the nonlinear functions $\mathbf{h}(\hat{\mathbf{x}}_n^{(i)})$ and $C(\hat{\mathbf{x}}_n^{(i)})$ and residual $\boldsymbol{\varepsilon}_n^{(i)}$ are evaluated with improving information. Performance analysis results (to be discussed shortly) suggest that two or three iterations are sufficient.

At time t_n, the same prior information $\bar{\mathbf{x}}_n$ and M_n, radar measurements $\mathbf{y}_n$, and measurement noise matrix R_n are used on each iteration step. M_n contains information that correlates errors in position states (which are directly observable from $\mathbf{y}_n$) with errors in velocity states and with errors in the bias states. As the filter gain matrix is proportional to these correlations, velocity and bias-state errors can be corrected with information in the position measurement residual.

VII. Performance Analysis

EKF(12) performance is demonstrated by Monte Carlo simulation of the recursive filter embedded in a truth model for the radar and the satellite orbit. A mobile phased-array radar tracks a satellite in a near-circular orbit. As the satellite traverses the sky, the radar array rotates in azimuth and elevation to maintain the satellite at or near array boresight. As the radar platform is mobile, radar position, velocity, orientation, and angular rate are provided by an INS mounted on the radar array near its boresight.

Radar measurement biases arise from uncompensated tropospheric refraction because real-time corrections to range and elevation (which are based on in situ measurements of pressure, temperature, and relative humidity) can remove all but 5–10% of the total clear-air refraction errors. Residual elevation errors scale with elevation, and the largest errors occur below 5° (refer to Fig. 1).

As discussed earlier, tropospheric bias error dynamics are modeled by a Markov process having a *variable* time constant τ_A that scales with elevation and (absolute) elevation rate (refer to Fig. 2). The elevation refraction error (Fig. 1) and its elevation gradient (the slope of the curve in Fig. 1) are implicit in τ_A. Although only absolute τ_A values are shown, positive τ_A values (stable response) occur with decreasing elevation, and negative τ_A values (unstable response) occur with decreasing elevation.

In weather environments, clouds can cause time-dependent refraction errors in range, elevation *and* azimuth. Time-dependent disturbances in range $\delta\rho$, elevation $\delta\gamma$ *and* azimuth $\delta\alpha$ are modeled by *colored noise*, or Gauss–Markov random processes with time constant τ_M:

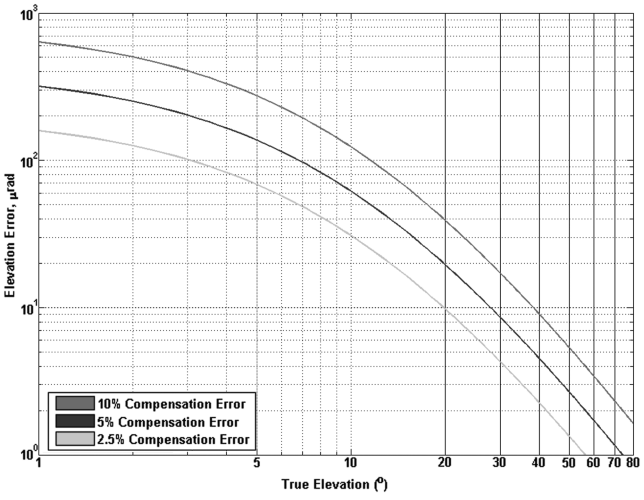

Fig. 1 Elevation errors caused by uncompensated tropospheric refraction depend on true elevation and error compensation accuracy.

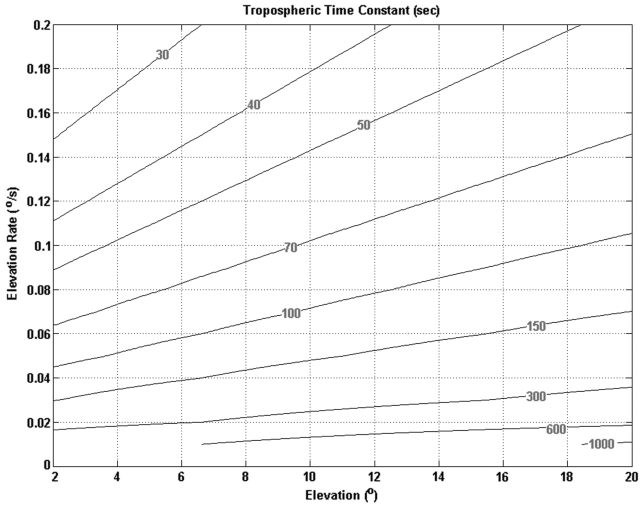

Fig. 2 Absolute tropospheric time constant $|\tau_A|$ (s) vs elevation and absolute elevation rate.

$$\frac{\mathrm{d}}{\mathrm{d}t}(\delta\rho)+\frac{1}{\tau_M}\delta\rho=\frac{1}{\tau_M}w_\rho,\qquad E\{w_\rho\}=0,\qquad E\{w_\rho^2\}=q_R$$

$$\frac{\mathrm{d}}{\mathrm{d}t}(\delta\gamma)+\frac{1}{\tau_M}\delta\gamma=\frac{1}{\tau_M}w_\gamma,\qquad E\{w_\gamma\}=0,\qquad E\{w_\gamma^2\}=q_\gamma$$

$$\frac{\mathrm{d}}{\mathrm{d}t}(\delta\alpha)+\frac{1}{\tau_M}\delta\alpha=\frac{1}{\tau_M}w_\alpha,\qquad E\{w_\alpha\}=0,\qquad E\{w_\alpha^2\}=q_\alpha$$

where w_R, w_γ, and w_α are white-Gaussian forcing functions with covariance statistics provided in Table 3. Covariance histories of the disturbances (refer to Fig. 3) are based on these models.

Table 3 Gauss–Markov tropospheric disturbance statistics

Gauss–Markov time constant τ_M	50 s
Range disturbance variance q_R	$(5\ \mathrm{m})^2$
Elevation disturbance variance q_γ	$(500\ \mu\mathrm{rad})^2$
Azimuth disturbance variance q_α	$(500\ \mu\mathrm{rad})^2$

Time-dependent INS misalignment biases are based on the linearized Euler equations provided in Sec. II and the initial condition statistics provided in Table 2. Although INS bias covariances do not fluctuate significantly (refer to Fig. 3), each yaw, pitch, and roll instantiation can fluctuate dramatically during radar elevation and azimuth steering maneuvers (not shown).

Without bias estimation, tropospheric refraction errors and INS misalignments cause EKF(6) orbit determination errors in position and velocity. Cross-range position (relative to the LOS) errors scale with the product of target range and angle error, whereas cross-range velocity errors scale with the product of range rate and angle error. As radar measurements are made in a rotating frame, Coriolis effects cause range rate errors that scale with the product of target range, angle error, and LOS angular rate (refer to Fig. 4). Tropospheric refraction errors dominate at low elevations (below 5°, occurring early and late in the track) whereas INS misalignment errors are important at higher elevations during the midtrack interval. Although position and velocity covariances usually underestimate the biased error statistics, covariance fidelity was improved (Fig. 4) with bias covariance models that *characterize*, but do not reduce the effects of, the bias errors. Nonzero velocity process noise ($q_v = 0.001\ \mathrm{m}^2/\mathrm{s}^3$) was required for EKF(6) to properly associate the biased detections with the track; otherwise a loss of track would have occurred midway through the satellite pass.

Analysis of the observability Grammian matrix indicates a full rank of 12, meaning that all the bias-state variables are mathematically observable. As noted earlier, 12-state observability

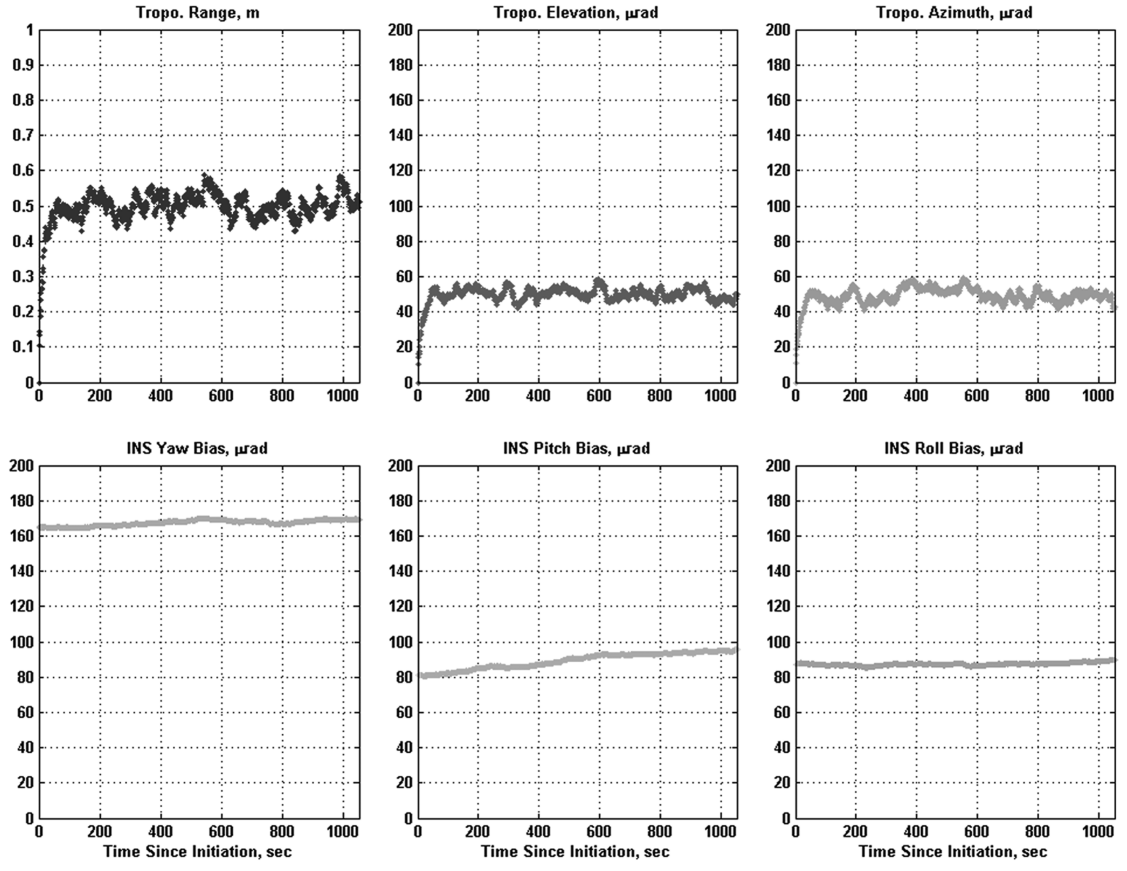

Fig. 3 1σ Gauss-Markov tropospheric biases and 1σ INS misalignment biases.

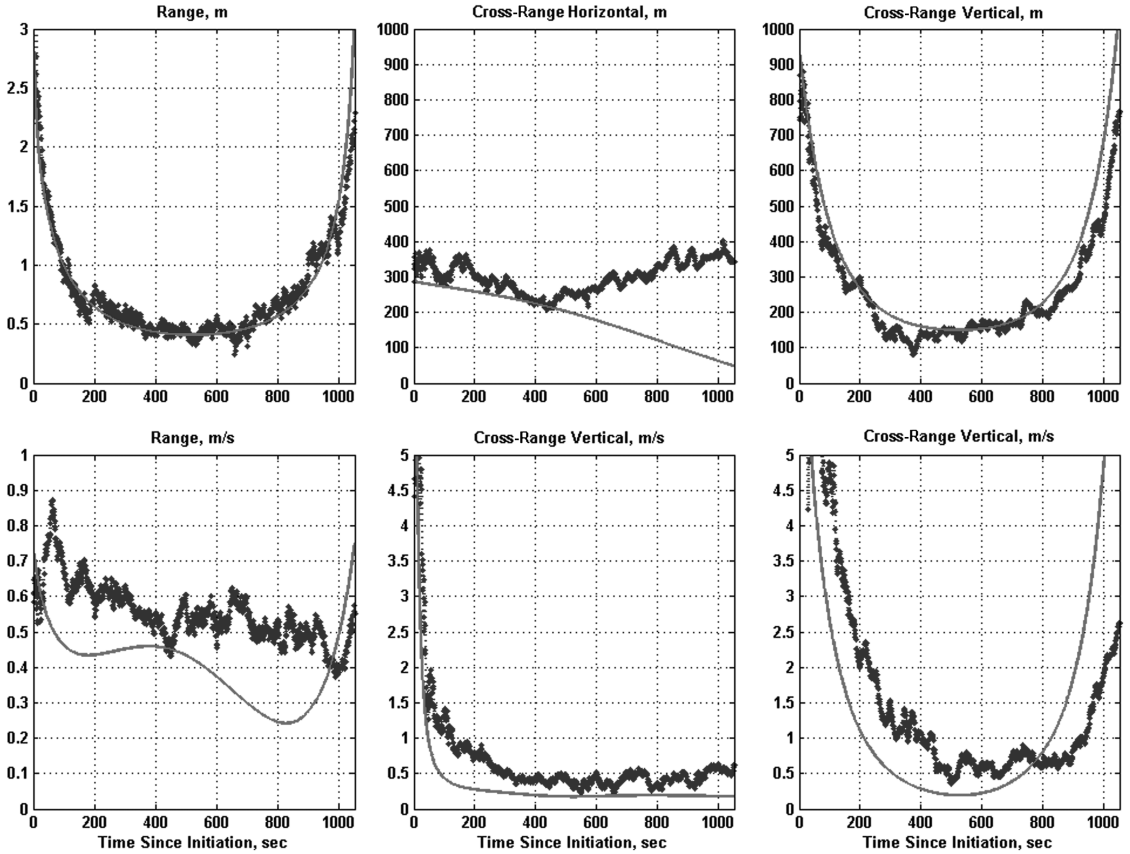

Fig. 4 Orbit determination 1σ accuracies and covariances without bias estimation (100 Monte Carlo trials).

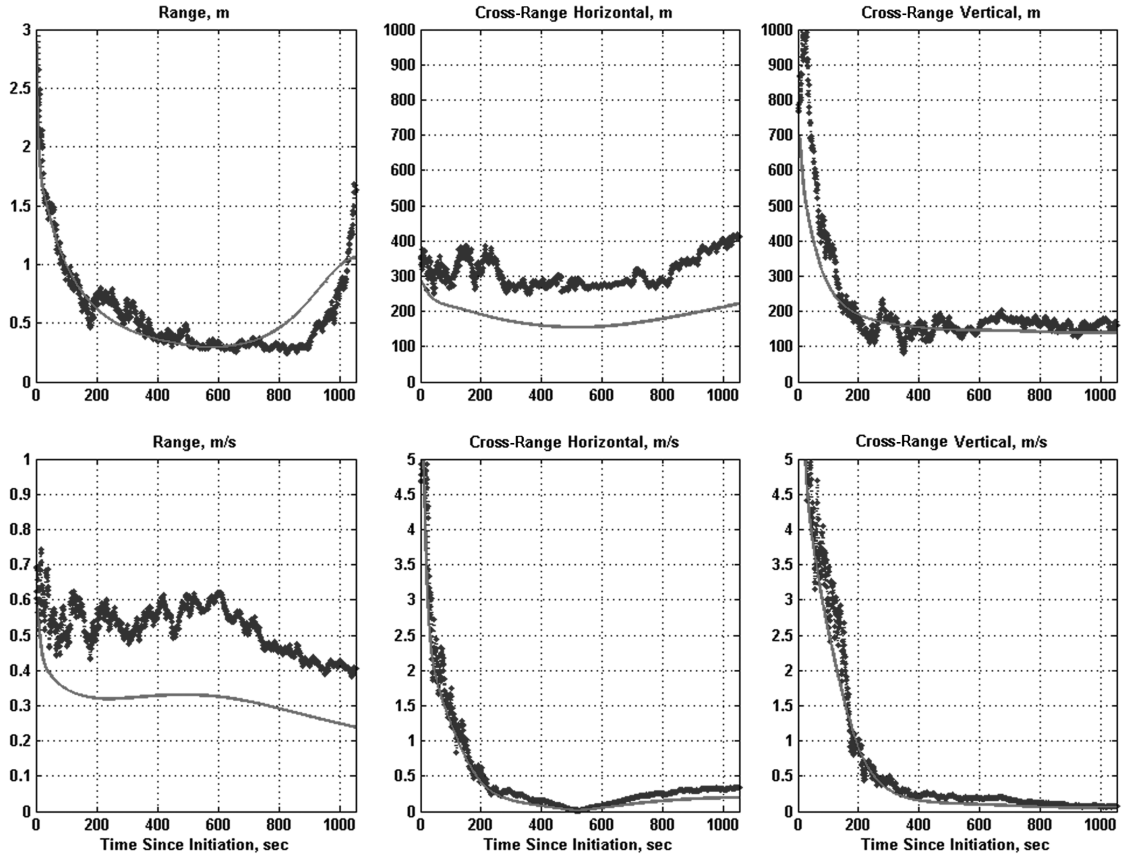

Fig. 5 Orbit determination 1σ accuracies and covariances with bias estimation (100 Monte Carlo trials).

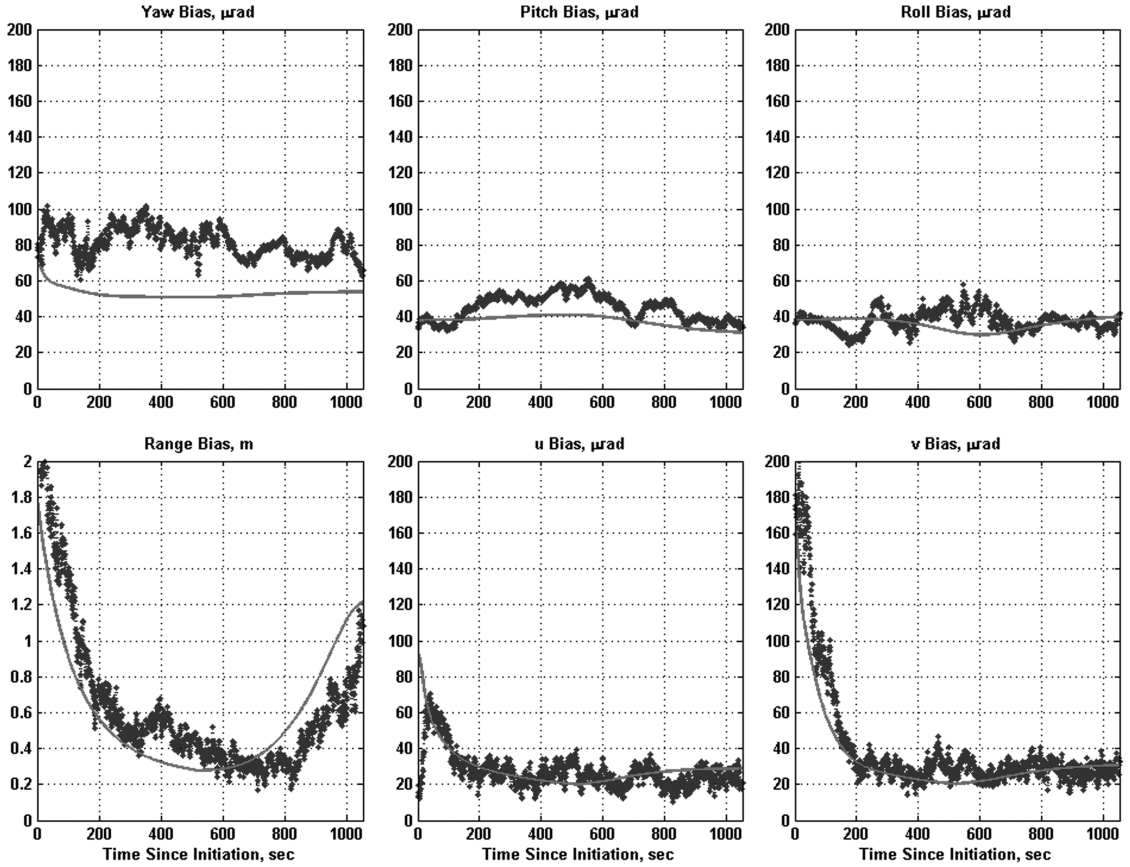

Fig. 6 Bias estimation 1σ accuracies and covariances (100 Monte Carlo trials).

is crucially dependent on inclusion of the second-order corrections to range associated with the misalignment biases, because the Grammian matrix would have rank 11 otherwise.

With bias estimation, the statistics of the position and velocity estimation errors are improved considerably (refer to Fig. 5). After the initial convergence interval, position and velocity errors can be reduced to and maintained at lower levels, particularly at low elevations toward the end of the track. The most dramatic error reductions occur in the cross-range–vertical error components, which are more observable than the cross-range–horizontal components. Residual errors in range rate scale with the product of satellite velocity and the root-sum-square yaw-pitch misalignments (Fig. 6). Moreover, the position and velocity covariances are more consistent with the track error statistics. The error statistics for the five angular bias states (refer to Fig. 6) show a twofold improvement compared to the input error statistics (Fig. 3).

VIII. Conclusions

An iterated EKF(12) was formulated for simultaneous (real-time) orbit determination and bias estimation. Orbit position and velocity states are estimated jointly with six dynamic (rather than static) bias states that model radar orientation biases and radar range-angle measurement biases. For steerable radar arrays that maintain the target near boresight, additional range-angle scale factor and misalignment errors are relatively unimportant and were not considered. Physical models for the bias dynamics and careful characterization of the bias influence in the measurement process provide bias-state observability and separability.

Orbit determination and bias estimation accuracies were demonstrated by Monte Carlo simulations. Without real-time bias estimation, INS misalignment and tropospheric biases can cause sizable position and velocity errors, particularly at low elevations. Moreover, the position and velocity covariances usually underestimate the biased error statistics, although covariance fidelity can be improved with bias covariance models that characterize, but do not reduce the size of, the bias errors. With real-time bias estimation, position and velocity errors can be reduced to and maintained at lower levels, particularly at low elevations, and covariance fidelity is markedly improved. Small velocity errors are clearly advantageous for track prediction and for cueing of other missile defense assets. Real-time bias estimation is thus needed for successful radar-to-radar track correlation and fusion.

Appendix: Tropospheric Time Constant

Clear-air (weather-free) tropospheric refraction causes elevation-dependent errors $\varepsilon(\gamma)$ in elevation and range that may be mathematically approximated by an exponential function:

$$\varepsilon(\gamma) = \varepsilon_0 e^{-b\gamma}$$

When ε_0 and b are constant parameters, the error time derivative may be expressed by

$$\dot{\varepsilon} = \frac{\mathrm{d}\varepsilon}{\mathrm{d}\gamma}\dot{\gamma} = -(b\dot{\gamma})\varepsilon$$

The quantity in parentheses may be replaced by an equivalent time constant:

$$\tau_A = \frac{1}{b\dot{\gamma}}$$

In reality, the gradient parameter

$$b = -\frac{1}{\varepsilon}\frac{\mathrm{d}\varepsilon}{\mathrm{d}\gamma}$$

is also elevation dependent because the error slope $\frac{\mathrm{d}\varepsilon}{\mathrm{d}\gamma}$ also depends on elevation. It follows that τ_A may be expressed by

$$\tau_A = -\frac{\varepsilon(\gamma)}{\dot{\gamma}\,\mathrm{d}\varepsilon/\mathrm{d}\gamma}$$

Acknowledgment

The author gratefully acknowledges the careful review, constructive criticism, and encouragement provided by Frederick E. Daum of the Raytheon Company, a pioneer in radar bias estimation.

References

[1] Okello, N., and Challa, S., "Joint Sensor Registration and Track-to-Track Fusion for Distributed Trackers," *IEEE Transactions on Aerospace and Electronic Systems*, Vol. 40, No. 3, July 2004, pp. 808–823.
doi:10.1109/TAES.2004.1337456

[2] Lin, X., and Bar-Shalom, Y., "Multisensor Target Tracking Performance with Bias Compensation," *IEEE Transactions on Aerospace and Electronic Systems*, Vol. 42, No. 3, July 2006, pp. 1139–1149.
doi:10.1109/TAES.2006.248212

[3] Friedland, B., "Treatment of Bias in Recursive Filtering," *IEEE Transactions on Automatic Control*, Vol. 14, No. 4, Aug. 1969, pp. 359–367.
doi:10.1109/TAC.1969.1099223

[4] Friedland, B., "Notes on Separate-Bias Estimation," *IEEE Transactions on Automatic Control*, Vol. 23, No. 4, Aug. 1978, pp. 735–738.
doi:10.1109/TAC.1978.1101789

[5] Alouani, A., Xia, P., Rice, T., and Blair, D., "On the Optimality of Two-Stage Estimation in the Presence of Random Bias," *IEEE Transactions on Automatic Control*, Vol. 38, No. 8, Aug. 1993, pp. 1279–1282.
doi:10.1109/9.233168

[6] Lerro, D., and Bar-Shalom, Y., "Bias Compensation for Improved Recursive Bearings-Only Target State Estimation," *Proceedings of the American Control Conference*, IEEE, Piscataway, NJ, June 1995, pp. 648–652.

[7] Myers, K., and Tapley, B., "Adaptive Sequential Estimation with Unknown Noise Statistics," *IEEE Transactions on Automatic Control*, Aug. 1976, pp. 520–523.
doi:10.1109/TAC.1976.1101260

[8] Tapley, B., *Statistical Orbit Determination*, Academic Press, New York, May 2004, pp. 387–438.

[9] "ARCHER Algorithm: Mathematical Development Paper and Implementation Concept Overview," Computer Sciences Corporation, Jan. 2004.

[10] Daum, F. E., and Huang, J., "Physics-Based Angle Bias Calibration of Wideband Radars," *Proceedings of the MDA Conference on Missile Defense-Sensors, Environment and Algorithms*, U.S. Army Night Vision & Electronic Sensors Directorate, Fort Belvoir, VA, Oct. 2004.

[11] Fitzgerald, R., "Effects of Range-Doppler Coupling on Chirp Radar Tracking Accuracy," *IEEE Transactions on Aerospace and Electronic Systems*, Vol. AES-10, No. 4, July 1974, pp. 528–532.
doi:10.1109/TAES.1974.307809

[12] Nickel, U., "Overview of Generalized Monopulse Estimation," *IEEE Aerospace and Electronics Systems Magazine*, Vol. 21, No. 6, June 2006, pp. 28–56.
doi:10.1109/MAES.2006.1662006

[13] Barton, D., *Modern Radar System Analysis*, Artech House, Norwood MA, 1988, pp. 533–552.

[14] Bean, B., "Comparison of Observed Tropospheric Refraction with Values Computed from the Surface Refractivity," *IRE Transactions on Antennas and Propagation*, July 1961, pp. 415–416.
doi:10.1109/TAP.1961.1145019

[15] Barton, D., *Modern Radar System Analysis*, Artech House, Norwood MA, 1988, pp. 302–310.

[16] Altshuler, E., "Tropospheric Range-Error Corrections for the Global Positioning System," *IEEE Transactions on Antennas and Propagation*, Vol. 46, No. 5, May 1998, pp. 643–649.
doi:10.1109/8.668906

[17] Hough, M. E., "Improved Performance of Recursive Tracking Filters Using Batch Initialization and Process Noise Adaptation," *Journal of Guidance, Control, and Dynamics*, Vol. 22, No. 5, Sept.–Oct. 1999, pp. 675–681.
doi:10.2514/2.4457

[18] Daum, F., and Fitzgerald, R., "Decoupled Kalman Filters for Phased Array Radar Tracking," *IEEE Transactions on Automatic Control*, Vol. 28, No. 3, March 1983, pp. 269–283.
doi:10.1109/TAC.1983.1103242

[19] Gelb, A. (ed.), *Applied Optimal Estimation*, MIT Press, Cambridge, MA, 1974, pp. 190–191.